

# Analysis of MEMS-Based Microneedles for Blood Monitoring

Adarsh Venkataraman Ganesan · Hardeep Kumar ·  
S. Swaminathan · K. K. Singh · Reenu Anne Joy ·  
Neeru Sood · Trupti Gokhale · R. K. Mittal

Published online: 7 February 2014  
© Springer Science+Business Media New York 2014

**Abstract** Diseases such as measles, mumps, rubella, chicken pox, etc. are diagnosed using blood. Once the patients are diagnosed with such diseases, it is necessary to periodically monitor their blood. Currently, the patients are hospitalized for blood monitoring. However, in the developing world where there is no access to hospitals, it is therefore necessary to have point-of-care devices for monitoring. In this paper, we present a novel biocompatible and robust design of microelectromechanical systems (MEMS)-based microneedle tailored for point-of-care blood monitoring. The cross-sectional areas of the needle bores were optimized, taking into the account of the bending stress on the needle and the flow rate in the channel. Ni and polyethylene glycol diacrylate (PEGDA) coatings are provided to the poly-Si microneedles to have better strength and biocompatibility, respectively. The mechanical and fluidic models of the microneedle were solved numerically using COMSOL Multiphysics 4.2a. Based on the computational results, the designed microneedle is found to have capability to extract blood at the rate of  $0.45 \mu\text{L/s}$  and, hence, be made available for blood monitoring.

**Keywords** MEMS · Blood monitoring · COMSOL · Microfabrication · Microneedles

## 1 Introduction

A major mission of clinical laboratories is to provide high-quality, efficient, timely laboratory testing to the health-care community at a reasonable cost. Each time when the laboratory support is provided, the quality, service, and cost are

considered. With the additional pressure that economics has created in health care today (managed care, Medicare, capitation), it has become a real challenge to meet these three criteria to accomplish the mission. Point-of-care technology (POCT) provides an opportunity to achieve these laboratory services at the same time. The shift from curative to preventative approaches to point of care are facilitated by the early detection with the help of microfluidic devices and lab-on-a-chip technology. Further several novel microscale technologies offer physicians a way to quickly assess patients' condition.

Diagnosis and monitoring of various disease conditions in the human body require just small volumes of blood. Extraction of small volumes of blood for such purposes has been a challenge in the last decade. The advent of the microelectromechanical systems (MEMS) technology has provided an innovative means of realizing micromachined hollow microneedles that can extract just microvolumes of fluids with minimal invasion of tissue and, hence, causing no pain. The practice of easy-to-use vaccination method through the microneedles is expected to replace injected vaccinations. In addition, the development of new vaccination systems to enable worldwide mass treatment is critical to evade pandemics of emerging infectious diseases such as severe acute respiratory syndrome.

## 2 Literature Review

Based on the fabrication methods, the microneedles are classified as in-plane where they are parallel to the substrate surface and out of plane where their length is protruded out of the substrate surface. There have been several reports wherein researchers have used the in-plane microneedles for activity recording and cellular chemostimuli of brain tissue [1]. On the other hand, Campbell et al. [2] have used out-of-plane microneedle array consisting of 100 microneedles with

---

A. V. Ganesan (✉) · H. Kumar · S. Swaminathan · K. K. Singh ·  
R. A. Joy · N. Sood · T. Gokhale · R. K. Mittal  
Dubai, United Arab Emirates  
e-mail: adarshvenkataraman@gmail.com

a length of 1.5 mm. The microneedles have been used to stimulate the visual cortex of the brain for sight treatment. Mukherjee et al. [3] demonstrated sampling of body fluids by capillary action achieved with 350- $\mu\text{m}$ -long hollow out-of-plane microneedles, which has subsequently been fabricated for microdialysis applications [4]. A majority of microneedles reported so in the literature are concerned with drug delivery in different applications. Most of the existing microfabrication technologies have been derived from processes developed to fabricate integrated circuits.

Aayogi et al. [5] proposed a fabrication method of microneedles with various tip angles made of biodegradable polymer (polylactic acid, referred to herein as PLA). They confirmed by the finite element method (FEM) simulation that the stress concentration occurs more severely at the tip area, as the needle becomes thin, and the tip angle becomes sharp and hence confirmed the effectiveness of sharp tip angle. Li et al. [6] reported the fabrication of a microneedle long enough to reach blood vessels and sharp enough to minimize nerve contact for minimally invasive blood extraction which is not met by using the traditional fabrication techniques.

Chen et al. [7] verified the microneedle-skin interactions using a nonlinear finite element model employing microbiomechanical properties of skin. Using that model, they discussed the influences of different geometries on microneedle fracture that could eventually help in optimizing the microneedle design. Hirobe et al. [8] developed an improved collagen-free microneedle patch, conducted clinical study, and evaluated its fundamental properties. Through the study, they also confirmed that the patch does not cause severe irritation.

Wing et al. [9] suggested that the microneedle pretreatment prior to the pilocarpine iontophoresis significantly increases the sweat production. Furthermore, they discussed that such results have the potential to improve the methodology currently used to diagnose cystic fibrosis and, more broadly, to administer drugs via the skin. Brogden et al. [10] found that adequate formation of the micropores is critical to the success of drug delivery technique, and hence, there is a need for monitoring micropores. In order to address this issue, they studied and confirmed that impedance measurements are suitable for use in both clinical and animal research environments to monitor the formation of new micropores. The design of microneedles and their fabrication steps are complicated in the abovementioned literature. In this paper, the authors propose easy-to-fabricate microneedles.

The paper is divided into three sections. In the first section, the materials of the microneedles were chosen in accordance to greater strength as well as biocompatibility, and the dimensions were chosen in accordance to the size of various blood components. The fabrication steps are also proposed.

In the second section, analyses were also performed to assess the failure of the microneedles. Microneedle showed an inverse relationship between their resistance to bending and

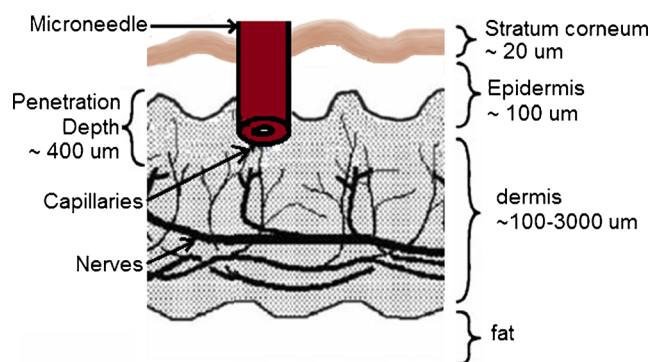


Fig. 1 Morphology of the human skin [12]

buckling stresses and their length. However, the maximum shear and compression force that they could withstand was independent of their length. In the last section, the average blood flow rate through the microneedle was calculated using computational fluid dynamics with the aid of COMSOL, and the blood extraction capability of the microneedle was tested. This was in terms of how quickly they could extract a 1- $\mu\text{L}$  sample of blood through a microneedle and fill a 25- $\mu\text{L}$  vessel. The effect of different RBC concentrations in the blood is also analyzed.

### 3 Microneedle Design Methodology

As shown in Fig. 1, blood vessels are typically present in the dermis at a depth of 150–3,000  $\mu\text{m}$  from the skin [11]. Accordingly, the microneedles have been designed for 250  $\mu\text{m}$  length. The range of the diameters of the blood corpuscles is from 2  $\mu\text{m}$  (platelets) to about 15  $\mu\text{m}$  (monocytes) [11]. Hence, to facilitate the passage of blood corpuscles, the diameter of circular cross section of the in-plane microneedle is chosen to be 30  $\mu\text{m}$ .

To take care of the biocompatibility issues of polysilicon as a material for biomedical use, a biocompatible material polyethylene glycol diacrylate (PEGDA) has been used as the

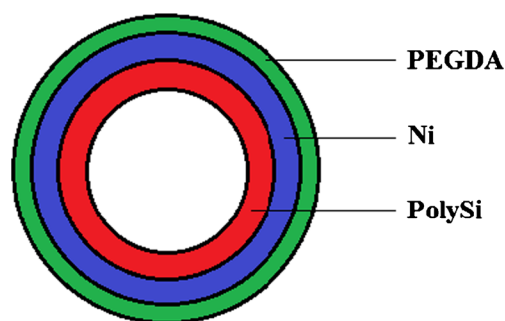
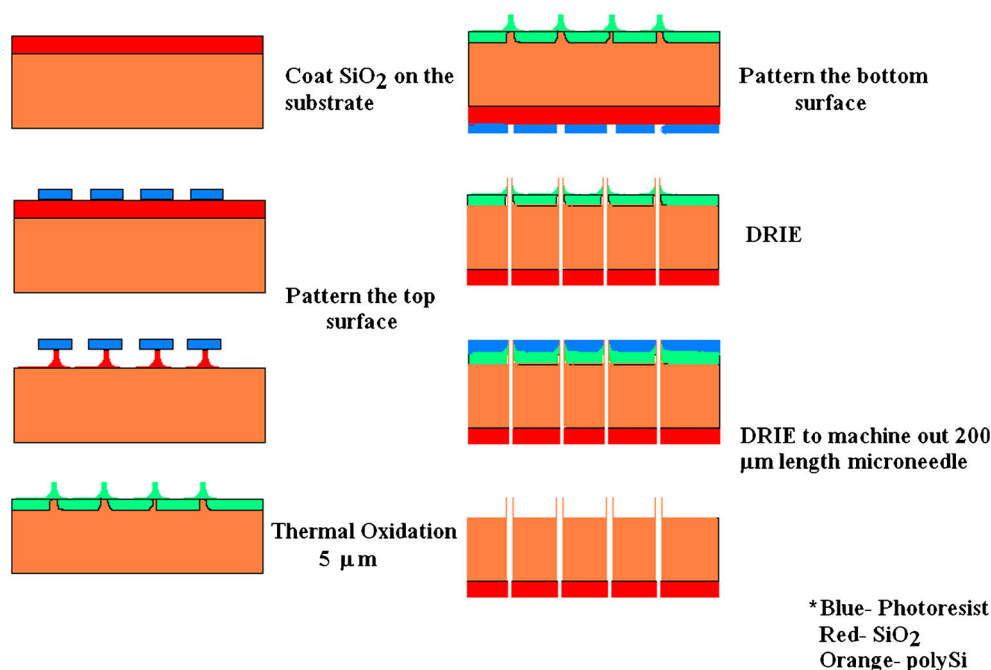


Fig. 2 Top view of the microneedle

**Fig. 3** Fabrication steps for the array of polysilicon microneedles



coating layer. PEGDA, owing to known biocompatibility [13] and FDA approval for human use, has a long history as nontoxic and nonimmunogenic polymer [14]. To increase the strength of the microneedle, a 10- $\mu\text{m}$  nickel has to be coated [15]. The schematic of the microneedle is shown in Fig. 2.

The polysilicon microneedles are fabricated through the steps given in Fig. 3. Further, Ni has to be coated onto the polysilicon microneedles. For this, an adhesion layer of chromium and gold has to be deposited by evaporation. First, 5 nm of chromium has to be deposited using a Veeco 401 resistance-heated evaporator. Then, without breaking vacuum, 100 nm of gold was then deposited. The needles have to be then flipped over and coated on the other side. The needles have to be electroplated in the nickel sulfate solution composed of 100 g/L nickel sulfate, 2.5 g/L nickel chloride, and 12.5 g/L boric acid. A DC current of 25 mA is at 23 °C for up to 30 min. The cathode current density is 30 mA/cm<sup>2</sup>. This will result in 10-mm-thick Ni coating on the needles [4]. The PEGDA polymer layer can be deposited onto the Ni coating by electro-deposition as given in the study by Roberts et al. [16].

**Table 1** Young's modulus of the skin layers

Layers	Young's modulus (MPa)
Stratum corneum (thickness, 0.015 mm)	330
Living epidermis (thickness, 0.080 mm)	17
Dermis (thickness, 1.1 mm)	1.7

#### 4 Failure Analysis of the Microneedle

A microneedle can fail under various stresses as it is pressed into the skin. These include failure by buckling, free bending, constrained bending, shear, and compression. In order to account for the anisotropy in stiffness and strength of a composite multilayer structure like that of our microneedle, the researchers have proposed many micromechanical failure theories. These failure theories are grouped into three sections. The first category is limit theory where the analysis is performed by comparing individual lamina stress or strain with corresponding strengths or ultimate strains. The second

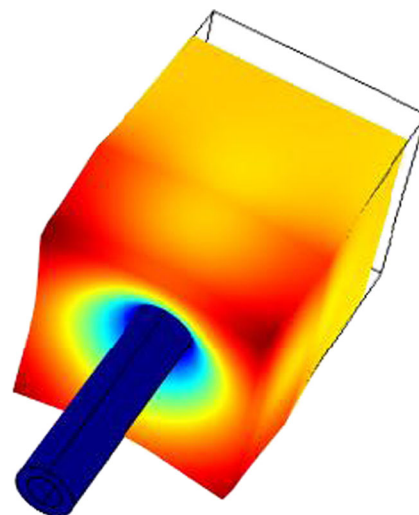
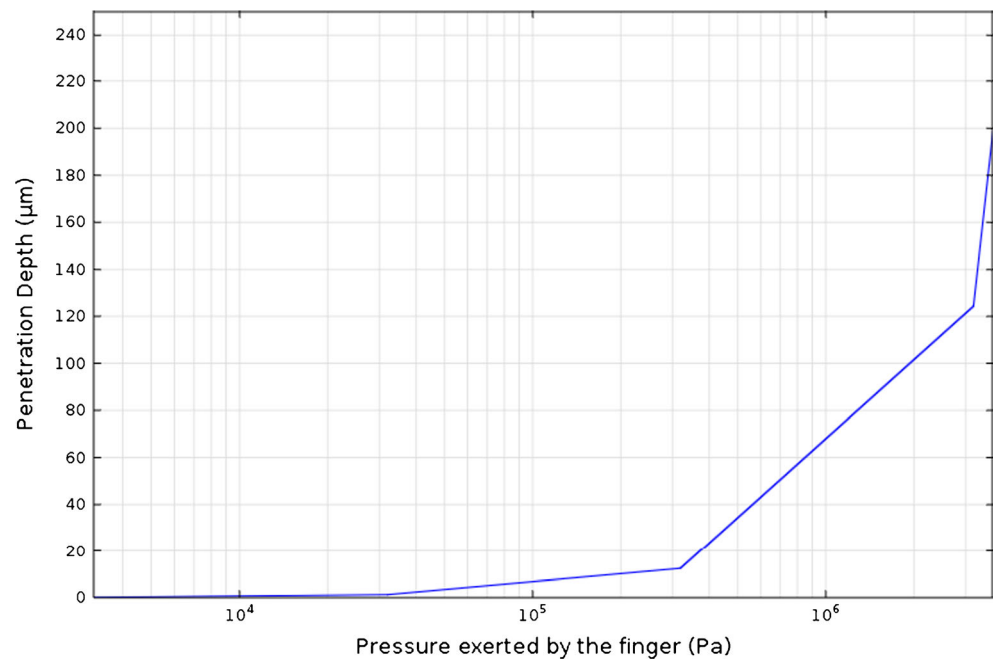


**Fig. 4** Penetration of the microneedle through the skin

**Fig. 5** Penetration depth vs. pressure exerted by the finger



category, i.e., interactive theory, involves the evaluation of overall expression in which all stress components are included. The overall failure is predicted without reference to particular failure modes. The last category deals with partially interactive theory which, in separate criteria, is imposed for fiber and interfiber failures [17].

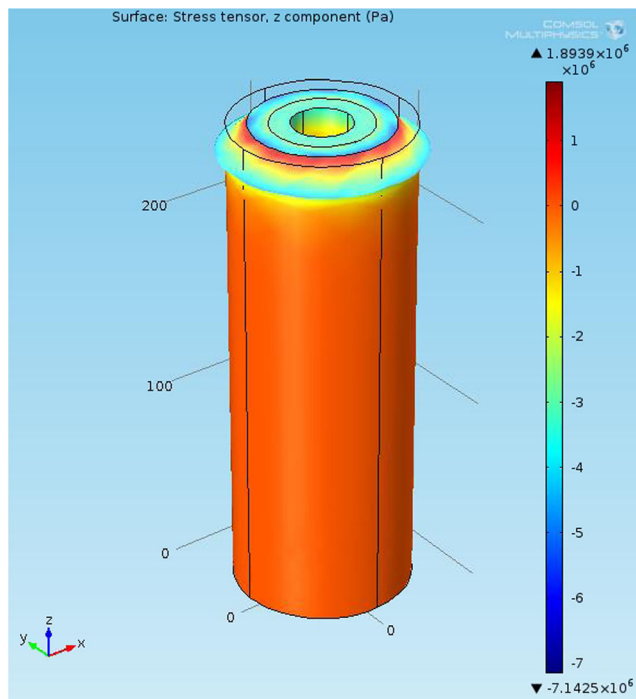


**Fig. 6** Stress distribution in the microneedle

Equations 1–5 [15] are used to calculate the magnitude of these forces on the microneedles.

$$F_{\text{Max buck}} = \frac{C\pi^2 EI}{L^2} \quad (1)$$

Here, the end condition constant  $C$  has a value of 0.25. It arises because each microneedle features a fixed joint, while its tip is a pivoted slider.  $E$  represents the Young's modulus,  $I$  is the needle's moment of inertia, and  $L$  is its length.

The maximum compressive force that each needle could withstand without breaking was calculated using Eq. 2:

$$F_{\text{Max compressive}} = \sigma_y A \quad (2)$$

where  $\sigma_y$  is the fracture strength of polysilicon, and  $A$  is the cross-sectional area of the capillary of a microneedle.

A microneedle will experience a bending moment when it just starts being inserted into skin. At this point, it can be modeled as a cantilever beam to imitate the maximum free bending it can withstand. After the needle has penetrated the skin, it cannot move laterally and will experience constrained

**Table 2** Coefficients values of Carreau model for different RBC concentrations of blood

Coefficients (%)	$\mu_{\text{inf}}$ (Pa/s)	$\mu_0$ (Pa/s)	$\lambda$ (s)	No.
25	2.57	17.8	12.448	0.33
45	3.45	161	39.42	0.3568
65	8.02	859.2	103.088	0.389

bending instead. The magnitude of free and constrained bending forces was found using the equations below:

$$F_{\text{Max free bend}} = \frac{\sigma_y I}{cL} \quad (3)$$

$$F_{\text{Max constrained bend}} = \frac{2\sigma_y I}{cL} \quad (4)$$

where  $c$  is the distance between the neutral axis and the external edge of the microneedle.

After a microneedle is inserted into the skin, it can move perpendicularly. This will induce a shear force, and the maximum shear force it can endure was calculated by means of Eq. 5:

$$F_{\text{Max shear}} = \frac{\sigma_y A}{2} \quad (5)$$

Equation 6 was used to calculate the minimum force needed to pierce skin with a microneedle of a given cross-sectional area.

$$F_{\text{Pierce}} = P_{\text{Pierce}} A \quad (6)$$

$P_{\text{Pierce}}$  represents the minimum pressure that is required to be applied on the microneedle to pierce the finger through the depth of 150  $\mu\text{m}$  (the point from where the blood vessels are present, beneath the skin, as shown in Fig. 1). In order to determine the value of  $P_{\text{Pierce}}$ , the mechanical model of the skin is designed. The Young's modulus values that are used in the skin model are listed in Table 1. Figure 4 shows the

deformation of the skin upon the microneedle penetration. Further, in Fig. 5, the relation between the penetration depth of the microneedle and its applied pressure is depicted.

From Fig. 5, the value of  $P_{\text{Pierce}}$  is found to be 3.18 MPa. The area moment of inertia  $I_{\text{Si}}$  of polysilicon is given by

$$I_{\text{Si}} = \frac{\pi}{64} (d_{\text{oSi}}^4 - d_{\text{iSi}}^4) \quad (7)$$

where  $d_{\text{oSi}}$  is the outer diameter of the polysilicon layer, and  $d_{\text{iSi}}$  is the inner diameter of the polysilicon layer.

Similarly, the area moment of inertia  $I_{\text{Ni}}$  of nickel is given by

$$I_{\text{Ni}} = \frac{\pi}{64} (d_{\text{oNi}}^4 - d_{\text{iNi}}^4) \quad (8)$$

where  $d_{\text{oNi}}$  is the outer diameter of the polysilicon layer and  $d_{\text{iNi}}$  is the inner diameter of the polysilicon layer.

From Fig. 2,  $d_{\text{oSi}} = d_{\text{iNi}} = 50 \mu\text{m}$ ,  $d_{\text{iSi}} = 30 \mu\text{m}$ ,  $d_{\text{oNi}} = 70 \mu\text{m}$ , and  $L = 250 \mu\text{m}$ .

Substituting the values of  $d_{\text{oSi}}$ ,  $d_{\text{iSi}}$ ,  $d_{\text{oNi}}$ , and  $d_{\text{iNi}}$  in Eqs. 7 and 8, we get  $I_{\text{Si}} = 2.670 \times 10^{-19} \text{ m}^4$  and  $I_{\text{Ni}} = 8.718 \times 10^{-19} \text{ m}^4$ , respectively.

Since  $E_{\text{PEGDA}} \ll E_{\text{Si}}$ , the PEGDA's contribution of area moment of inertia is not considered. The needle's area moment of inertia  $I$  is given by

$$I = \frac{E_{\text{Si}} \times I_{\text{Si}} + E_{\text{Ni}} \times I_{\text{Ni}}}{E_{\text{Si}}} \quad (9)$$

Substituting  $E_{\text{Si}} = 160 \text{ GPa}$  and  $E_{\text{Ni}} = 219 \text{ GPa}$  in Eq. 11, we get  $I = 1.460 \times 10^{-10} \text{ m}^4$ . Based on the dimensions, the inner cross-sectional area of microneedle is found to be  $5.6548 \times 10^{-9} \text{ m}^2$ .

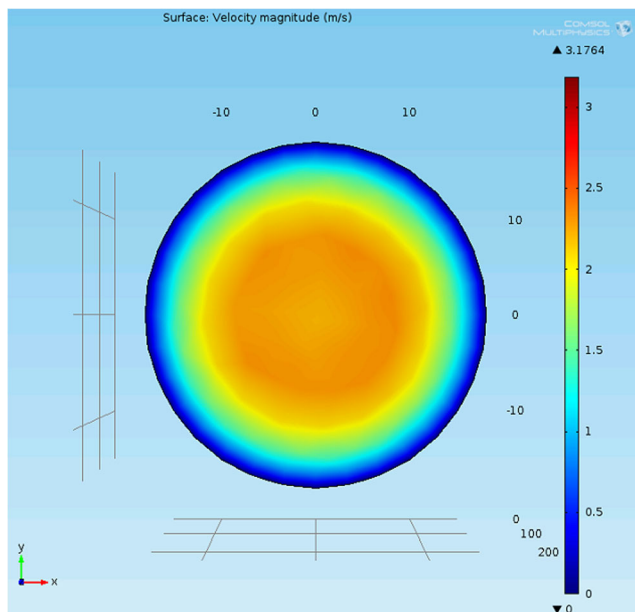


**Fig. 7** Bulk velocity profile of blood (25 % RBC) flow at the outlet

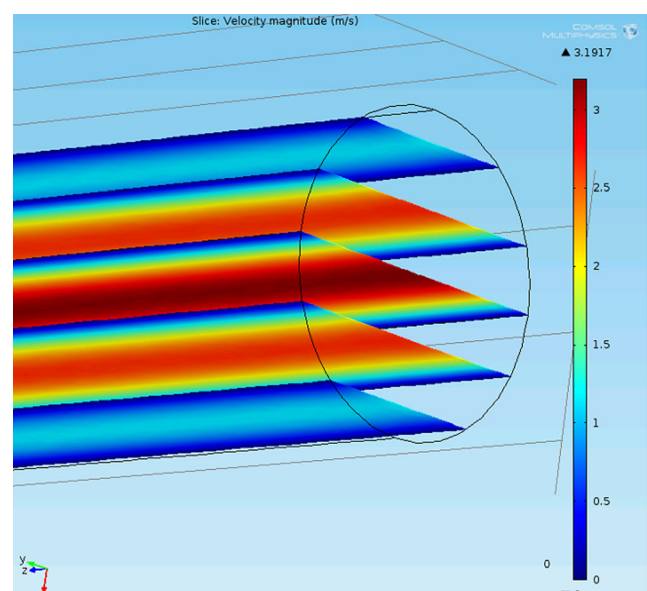
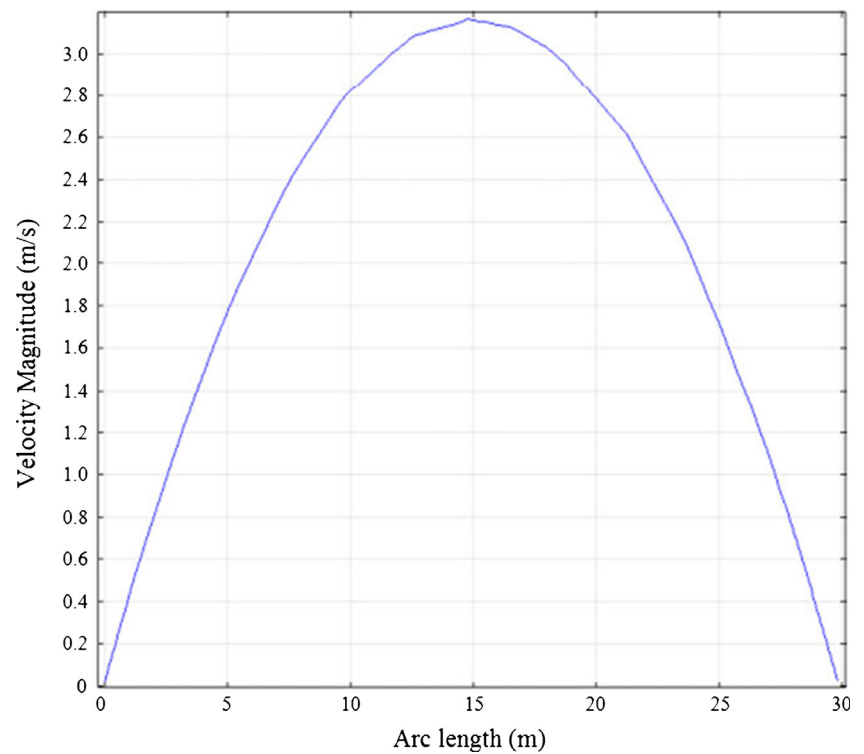


**Fig. 8** Bulk velocity profile across the length of the microneedle



**Fig. 9** Bulk velocity magnitude across the diameter of microneedle



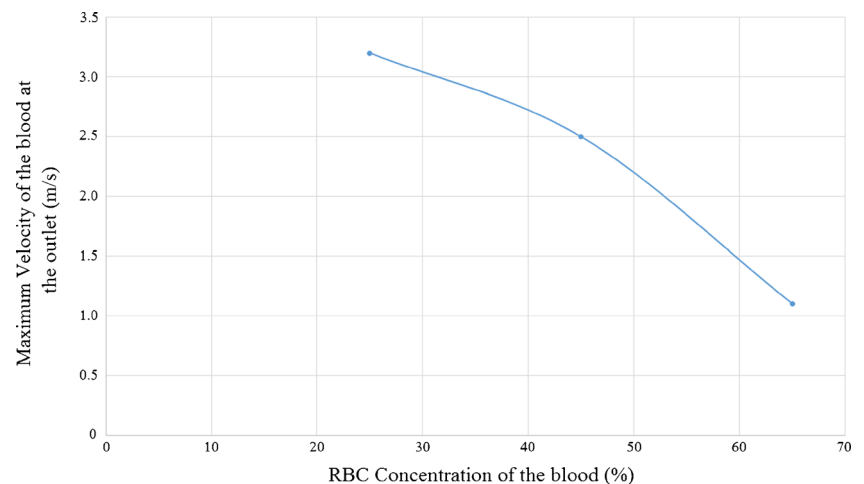
Using the above equations, hence, the maximum buckling force, maximum compressive force, maximum free bending force, maximum constrained force, and maximum shear force are found to be  $3.0279 \times 10^5$ , 6.7858, 0.1557, 0.3114, and 3.3929 N, respectively.

However, from Eq. 6, it is found that the minimum force needed to pierce the skin is 0.01798 N. Since all the forces are

substantially larger than the skin resistance force, microneedle should be able to pierce the skin without breaking. To verify the results, the microneedle was also simulated in COMSOL Multiphysics. The result of the same is shown in Fig. 6.

The simulation results show that the stress on the tip of polysilicon is much lesser than their yield strengths, i.e.,

**Fig. 10** Maximal bulk velocity of the blood at the outlet for different RBC concentrations



1.2 GPa. Therefore, the microneedle is strong enough to withstand the pressure of 3.181 MPa.

## 5 Blood Flow Simulations

The blood flow in microneedle has been studied numerically using the Carreau model that incorporates shear thinning non-Newtonian viscosity of blood. In the Carreau model, the viscosity of a non-Newtonian fluid is dependent upon shear rate ( $\delta\gamma/\delta t$ ).

$$\mu = \mu_{\text{inf}} + (\mu_0 + \mu_{\text{inf}})[1 + (\lambda\dot{\gamma})^2]^{\frac{n-1}{2}} \quad (10)$$

The properties of blood for different RBC concentrations are listed in Table 2.

The boundary conditions for the simulation are the following:

1.  $P_{\text{in}} = P_{\text{out}} = P_{\text{atm}}$
2. Slip conditions on the walls.

The microfluidic channel dimensions are optimized based on the maximum blood filling distance. The maximum blood filling distances are obtained for different diameters of microneedles and for different RBC concentrations.

In the slip flow regime, the slip velocity term is also involved and is proportional to the shear rate and given by [18]

$$\bar{u}_s = \gamma L_s \quad (11)$$

where  $\gamma$  is the shear rate, and  $L_s$  is the slip length of blood. The relative axial velocity is, hence, given by  $U = u + \bar{u}_s$ , where  $u$  is the bulk velocity of the blood. Based on the appropriate calculations, the slip velocity is found out to be 5 % of the bulk velocity.

The following PDE is solved to get the bulk velocity profile for the blood in the channel (Figs. 7, 8, and 9).

$$\rho(u \cdot \nabla)u = \nabla \cdot [-pI + \mu(\nabla u + (\nabla u)^T) - \frac{2}{3}\mu(\nabla \cdot u)I] \quad (12)$$

where  $p$  is the pressure at the inlet,  $\rho$  is the density of the blood, and  $\mu$  is the dynamic viscosity of the blood. The following boundary conditions are applied at the inlet and the outlet.

$$p = p_0, \left[ \mu(\nabla u + (\nabla u)^T) - \frac{2}{3}\mu(\nabla \cdot u)I \right] \hat{n} = 0 \quad (13)$$

The variation of velocity profile with RBC concentration was also found out using the same model, and the results are shown in Fig. 10.

$$Q = \int_{x=0}^R U \times \pi \times (2 \times x) dx \quad (14)$$

By using the equation, the volumetric flow rate of blood in the microneedle was found out to be 0.45  $\mu\text{L/s}$ .

## 6 Conclusions

The aim of this paper was to evaluate the possibility of using microneedles for blood monitoring, and this has been strongly confirmed through conducting a literature review as well as mechanical stress and blood flow simulations. In this study, five mechanical stresses which microneedles can experience when piercing the skin were modeled, plus simulations of blood flow through a capillary were conducted. The designed microneedle has been analyzed and found to effectively draw 1  $\mu\text{L}$  of blood with 25 % RBC concentration with a contact time of 2.23 s; and hence paving way for quick monitoring.

## References

1. Griss, P., et al. (2003). Side-opened out of plane microneedles for microfluidics transdermal liquid transfer. *Journal of Microelectromechanical Systems*, 12(3), 296–301.
2. Campbell, P. K., et al. (1991). A silicon-based, three-dimensional neural interface: manufacturing processes for an intracortical electrode array. *IEEE Transactions on Biomedical Engineering*, 38(8), 758–768.
3. Mukherjee, E. V., et al. (2001). Microneedle array for transdermal biological fluid extraction and in situ analysis. *Sensors and Actuators A*, 114, 267–275.
4. Zahn, J. D., et al. (2004). Continuous on-chip micropumping for microneedle enhanced drug delivery. *Biomedical Microdevices*, 6(3), 183–190.
5. Aoyagi, S., Izumi, H., Fukuda, M. (2008). Biodegradable polymer needle with various tip angles and consideration on insertion mechanism of mosquito's proboscis. *Sensors and Actuators A*, 143, 20–28.
6. Li, C. G., Lee, C. Y., Lee, K., Jung, H. (2013). An optimized hollow microneedle for minimally invasive blood extraction. *Biomedical Microdevices*, 15, 17–25.
7. Chen, S., Li, N., Chen, J. (2012). Finite element analysis of microneedle insertion into skin. *Micro and Nano Letters*, 7(12), 1206–1209.
8. Hirobe, S., Azukizawa, H., Matsuo, K., Zhai, Y., Quan, Y.-S., Kamiyama, F., et al. (2013). Development and clinical study of a self-dissolving microneedle patch for transcutaneous immunization device. *Pharmres*, 13, 1092–1096.

9. Wing, D., Prausnitz, M. R., Buono, M. J. (2013). Skin pretreatment with microneedles prior to pilocarpine iontophoresis increases sweat production. *Clin Physiol Funct Imaging*, 33, 436–440.
10. Brogden, N. K., Ghosh, P., Hardi, L., Crofford, L. J., Stinchcomb, A. L. (2013). Development of in vivo impedance spectroscopy techniques for measurement of micropore formation following microneedle insertion. *Journal of Pharmaceutical Sciences*, 102(6), 1948–1956.
11. Barrett, K. E., et al. (2009). *Ganong's review of medical physiology* (23rd ed.). New York: McGraw-Hill.
12. Gattiker, G. E., Kaler, V. I. S. K., Mintchev, M. P. (2005). Electronic mosquito: designing a semi-invasive microsystem for blood sampling, analysis and drug delivery applications. *Microsystem Technologies*, 12, 44.
13. Sun, G., & Chu, C.-C. (2006). Synthesis, characterization of biodegradable dextran-allyl isocyanate-ethylamine/polyethylene glycol-diacrylate hydrogels and their in vitro release of albumin. *Carbohydrate Polymers*, 65, 273–287.
14. Pasut, G., & Veronese, F. M. (2007). Polymer-drug conjugation, recent achievements and general strategies. *Progress in Polymer Science Oxford*, 32, 933–961.
15. Zahn, J. D., et al. (2000). Microfabricated polysilicon microneedles for minimally invasive biomedical devices. *Biomedical Microdevices*, 2(4), 295–303.
16. Roberts, M., et al. (2011). 3D lithium ion batteries—from fundamentals to fabrication. *Journal of Materials Chemistry*, 21(27), 9876–9890.
17. Sandhu, R.S. (1972). A survey of failure theories of isotropic anisotropic materials, AFFDL-TR-72-71, AD 756889. Technical report. Air Force Flight Dynamics Laboratory, Wright-Patterson Air Force Base.
18. Gad-el-Hak, M. (2005). Differences between liquid and gas transport at the microscale. *Technical Sciences* 53(4).